distribution of atomic velocities in the beam causes a spread (of $\approx 2$ ms) in the time of flight between the interaction region and the probe region. This, along with the finite bandwidth of the PD, leads to a reduction of the signal-modulation contrast (see below). The choice of the modulation frequency of 76.2 Hz is a tradeoff between this contrast degradation and the frequent E-field reversal.

## VI. RESULTS AND ANALYSIS

In Fig. 7 a profile of the B-field-split 408-nm spectral line of the $^{174}$Yb is shown. The 649-nm-light-induced fluorescence was recorded during a single profile scan. Statistical error bars determined directly from the spread of data are smaller than the points in the figure. The peculiar asymmetric line shape of the Zeeman components is a result of the dynamic Stark effect [7]. During a typical

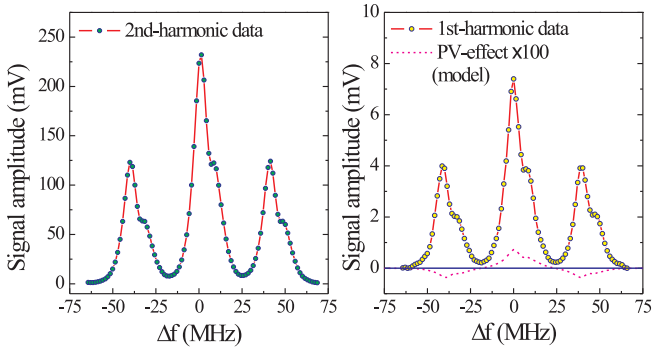


FIG. 7: (color online) A profile of the B-field-split 408-nm spectral line of $^{174}$Yb recorded at 1st- and 2nd-harmonic of the modulation. Also shown is a simulated PV contribution in the first-harmonic signal. $\tilde{E}$=5 kV/cm; DC offset=40 V/cm; $\theta = \pi/4$; the effective integration time is 200 ms per point.

experimental run 100 profiles are recorded for each combination of the magnetic field and the polarization angle (400 profile scans in total). In order to compute the normalized amplitude, $r_q$, of a selected Zeeman component, the actual first-harmonic signal near the Zeeman peak is divided by the respective second-harmonic signal and then averaged over a number of the data points[1]. Then, the combination $\mathcal{K}$ of Eq. (14) is computed for each profile scan followed by averaging the result over all the scans at a given B-$\theta$ configuration. This procedure is repeated for all four reversals, and all B-$\theta$ symmetrical contributions, $\mathcal{K}_{1-4}$, are determined. In the present experiment, the values of $\mathcal{K}_{2,3,4}$-terms are found to be consistent with zero within the statistical uncertainty, which is the same as that of the PV-asymmetry (see below).

As can be seen from Table II, terms in $\mathcal{K}_1$ associated with the fields imperfection are of crucial importance:

$$\frac{16}{\tilde{E}_0}\left[e_y\left(\frac{\tilde{e}_z}{2\tilde{E}_0}+\frac{\tilde{b}_x}{B}\right)+e_z\frac{\tilde{e}_y}{2\tilde{E}_0}\right].$$

In order to measure the contribution of these terms, artificially exaggerated E-field imperfections both static and oscillating, $e_z^{ex}$, $e_y^{ex}$, $\tilde{e}_y^{ex}$ and $\tilde{e}_z^{ex}$, are imposed by use of the "correction electrodes" (see Fig. 6), and two sets of the experiments were performed. In the first one, a DC-voltage was applied to the correction electrodes, and the measurements were done reversing $e_y^{ex}$ and $e_z^{ex}$. These experiments yield values of $\tilde{e}_y$ and $\tilde{e}_z + 2\tilde{E}_0\tilde{b}_x/B$. In the second set, an AC-voltage modulated synchronously with the main E-field is applied to the correction electrodes. In order to reverse the sign of the parasitic terms a $\pi$-phase-shift of $\tilde{e}_y^{ex}$ and $\tilde{e}_z^{ex}$ with respect to the modulation signal is employed by switching the wiring of the correction electrodes. Thus, values of the DC-imperfections, $e_y$ and $e_z$, are determined. The magnitudes of the applied electric fields and their distributions are calculated using a 3D-numerical-model of the interaction region. The results of the experiments are presented in Table III. The

TABLE III: Results of measurements of the electric field imperfections using artificially exaggerated AC- and DC-components, $\tilde{e}_{y,z}^{ex}$ and $e_{y,z}^{ex}$. These fields were generated by use of the correction electrodes, Fig. 6. $\tilde{E}_0 = 2000(2)$ V/cm.

| **DC-Set** | **AC-Set** |
|---|---|
| Exaggerated imperfections (V/cm) | |
| $e_y^{ex} = -140(2)$ | $\tilde{e}_y^{ex} = -120(2)$ |
| $e_z^{ex} = 20(2)$ | $\tilde{e}_z^{ex} = 30(2)$ |
| Measurements (mV/cm) | |
| $\tilde{e}_y\frac{e_z^{ex}}{2\tilde{E}_0} = 16(10)$ | $e_y\frac{\tilde{e}_z^{ex}}{2\tilde{E}_0} = 4(5)$ |
| $(2\tilde{E}_0\frac{\tilde{b}_x}{B}+\tilde{e}_z)\frac{e_y^{ex}}{2\tilde{E}_0} = 442(10)$ | $e_z\frac{\tilde{e}_y^{ex}}{2\tilde{E}_0} = 40(5)$ |
| Parasitic fields (V/cm) | |
| $\tilde{e}_y = 3.2(2)$ | $e_y = 0.5(0.6)$ |
| $(2\tilde{E}_0\frac{\tilde{b}_x}{B}+\tilde{e}_z) = -12.6(0.3)$ | $e_z = -1.3(0.2)$ |

net contribution of these imperfections to $\mathcal{K}_1$ in the absence of the exaggerated fields is found to be [2]:

$$e_y\left(\frac{\tilde{e}_z}{2\tilde{E}_0}+\frac{\tilde{b}_x}{B}\right)+e_z\frac{\tilde{e}_y}{2\tilde{E}_0} = \\ = -2.6(1.6)_{\text{stat.}}(1.5)_{\text{syst.}}\ \text{mV/cm}. \qquad (21)$$

[1] In the normalized rate calculations only data points having intensity higher that 1/3 of the respective Zeeman peak are used to avoid excessive noise from spectral regions with low signal intensity.

[2] Compare with the PV asymmetry parameter $\zeta/\beta \approx 40$ mV/cm.